NANO LETTERS

Letter

Cite This: Nano Lett. 2019, 19, 5725−5731

pubs.acs.org/NanoLett

# Resolving the Correlation between Tip-Enhanced Resonance Raman Scattering and Local Electronic States with 1 nm Resolution

Shuyi Liu,[†] Melanie Müller,[†] Yang Sun,[‡] Ikutaro Hamada,[‡,§] Adnan Hammud,[∥] Martin Wolf,[†] and Takashi Kumagai*[,†,⊥]

[†]Department of Physical Chemistry, Fritz-Haber Institute of the Max-Planck Society, Faradayweg 4-6, 14195 Berlin, Germany

[‡]Global Research Center for Environment and Energy Based on Nanomaterials Science, National Institute for Materials Science, 1-1 Namiki, Tsukuba, Ibaraki 305-0044, Japan

[§]Department of Precision Science and Technology, Graduate School of Engineering, Osaka University, 2-1 Yamada-Oka Suita, Osaka 565-0871, Japan

[∥]Department of Inorganic Chemistry, Fritz-Haber Institute of the Max-Planck Society, Faradayweg 4-6, 14195 Berlin, Germany

[⊥]JST-PRESTO, 4-1-8 Honcho, Kawaguchi, Saitama 332-0012, Japan

Supporting Information

**ABSTRACT:** Low-temperature tip-enhanced Raman spectroscopy (TERS) enables chemical identification with single-molecule sensitivity and extremely high spatial resolution even down to the atomic scale. The large enhancement of Raman scattering obtained in TERS can originate from physical and/or chemical enhancement mechanisms. Whereas physical enhancement requires a strong near-field through excitation of localized surface plasmons, chemical enhancement is governed by resonance in the electronic structure of the sample, which is also known as resonance Raman spectroscopy. Here we report on tip-enhanced resonance Raman spectroscopy (TERRS) of ultrathin ZnO layers epitaxially grown on a Ag(111) surface, where both enhancement mechanisms are operative. In combination with scanning tunneling spectroscopy (STS), it is demonstrated that the TERRS intensity strongly depends on the local electronic resonance of the ZnO/Ag(111) interface. We also reveal that the spatial resolution of TERRS is dependent on the tip−surface distance and reaches nearly 1 nm in the tunneling regime, which can be rationalized by strong-field confinement resulting from an atomic-scale protrusion on the tip apex. Comparison of STS and TERRS mapping clearly shows a correlation between resonantly enhanced Raman scattering and the local electronic states at near-atomic resolution. Our results suggest that TERRS is a new approach for the atomic-scale optical characterization of local electronic states.

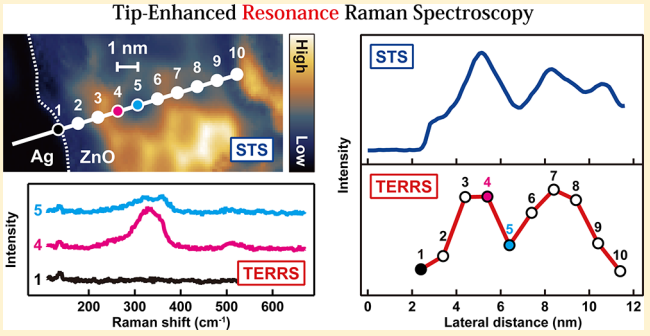


**KEYWORDS:** *Tip-enhanced Raman spectroscopy, resonance Raman scattering, scanning tunneling microscopy, ultrathin ZnO layer*

Raman scattering is an inelastic process mediated by the interaction between light and matter (e.g., molecules) typically via vibrational excitation/de-excitation. Raman spectroscopy is employed as a powerful tool for chemical analysis in a broad range of fundamental and applied science. However, due to the very small Raman cross section chemical identification at the single-molecule level had been unfeasible for a long time since the discovery of the Raman effect in 1928. In the late 1970s, it was found that Raman scattering is strongly enhanced for molecules adsorbed on rough surfaces of coinage metals,[1] a process known as surface-enhanced Raman scattering (SERS). This effect has been demonstrated to possess a single-molecule detection capability by using metallic nanoparticles.[2] In SERS, two different enhancement mechanisms have been generally discussed, namely, physical and chemical enhancement. The former mechanism is attributed to strong electromagnetic field enhancement through surface plasmon excitation in metallic nanostructures. The latter mechanism is associated with resonances in the electronic structure of an adsorbate−surface complex.

Since the early 2000s, tip-enhanced Raman spectroscopy (TERS) has emerged as a powerful analytical tool in nanoscale science and technology,[3−5] combining the chemical sensitivity of SERS with the high-spatial resolution of scanning probe microscopy (SPM).[6−8] More recently, TERS in a well-defined environment, that is, low-temperature and ultrahigh-vacuum (UHV) conditions, has become available,[9−11] providing microscopic insights into underlying mechanisms of enhanced Raman scattering processes. It is a general consensus that both physical and chemical enhancement are required to dramat-

Received: June 10, 2019
Revised: July 12, 2019
Published: July 30, 2019

ically enhance TERS signals.[6] For chemical enhancement (resonance Raman scattering) the local electronic structure of the sample should have a considerable impact, which can be examined by combining scanning tunneling spectroscopy (STS) with TERS. It is an intriguing question how the confined electromagnetic field interacts with local electronic states because it is associated with the basic principle of near-field optical spectroscopy as well as fundamental physics of light−matter interaction at the nanoscale. However, an explicit correlation between local electronic states and TERS signals has not been demonstrated. Here, we report tip-enhanced resonance Raman scattering (TERRS) of ultrathin ZnO layers epitaxially grown on a Ag(111) surface, where both physical and chemical enhancement are involved in the process. The ZnO layer serves as a robust and intriguing model system for TERRS as the electronic structure is dependent on the layer thickness and nanoscale corrugation of the local density of states (DOS) occurs due to a subtle structural mismatch with the Ag surface.[12] Moreover, we also show that the spatial resolution of TERRS depends on the tip−surface distance and reaches ∼1 nm in the tunneling regime, allowing to correlate the TERRS intensity with the local DOS at near-atomic resolution.

Figure 1a shows an STM image of 2- and 3-monolyer (ML) ZnO on the Ag(111) surface. The periodic protrusions in the ZnO layers correspond to a Moiré pattern resulting from a lattice mismatch between the ZnO and Ag(111), as depicted in Figure 1b.[12] The 2-ML ZnO has a (0001) orientation with a flat geometry like hexagonal boron nitride, whereas it relaxes to the wurtzite structure in thicker ZnO layers.[13] Previous studies suggest that this structural change occurs (partially) already at 3 ML.[14−16] Figure 1c shows TERRS spectra obtained using an Au tip on 2-ML ZnO with 633 nm excitation at different laser fluences, exhibiting the characteristic vibrational peaks. No Raman signal of the ZnO layer is observed in the far-field spectrum (see Supporting Information). As shown in the inset of Figure 1c, the Raman intensity ($I_R$) linearly depends on the laser fluence ($F$), indicating spontaneous Raman scattering. The TERRS signal from 2-ML ZnO can be obtained with both Au or Ag tips at 633 nm excitation. The intense peaks around 350 $cm^{-1}$ are assigned to out-of-plane optical phonon modes of the ZnO layer, which can be largely enhanced according to the surface selection rule,[17,18] whereas the weak peaks at 508 and 573 $cm^{-1}$ belong to in-plane modes according to density functional theory calculations of free-standing 2-ML ZnO[19,20] and at a 2-ML ZnO/Ag(111) interface (see Supporting Information for details).

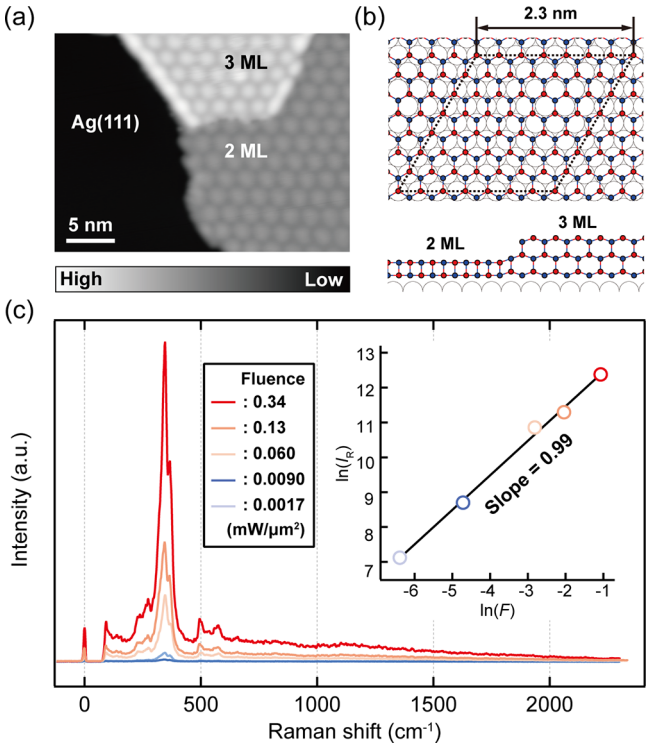


**Figure 1.** TERRS of 2-ML ZnO on Ag(111). (a) STM image of the ZnO layers on the Ag(111) surface ($V_{bias}$ = 1 V, $I_t$ = 100 pA). (b) Schematic model of the ZnO layer on Ag(111). The black dashed rhomboid indicates the ZnO(0001)-(7 × 7)/Ag(111)-(8 × 8) coincidence structure. (c) TERRS spectrum of 2-ML ZnO at different fluences (Au tip, $\lambda_{ext}$ = 633 nm, $F$ = 0.38 mW $\mu m^{-2}$, $V_{bias}$ = 1 V, $I_t$ = 1 nA, exposure time ($t_{exp}$) = 300 s, 78 K). The inset shows the fluence dependence of the TERRS intensity ($I_R$) at 345 $cm^{-1}$. The data are fitted by the power raw dependence $I \propto P^N$, and $N$ = 0.99 ± 0.01 is obtained.

The physical enhancement mechanism in TERS is governed by localized surface plasmon resonance (LSPR) in the junction. We observed a clear correlation between the TERRS intensity and the LSPR using scanning tunneling luminescence (STL) in which LSPR is excited by inelastic scattering of tunneling electrons.[21] Figure 2a shows the STL

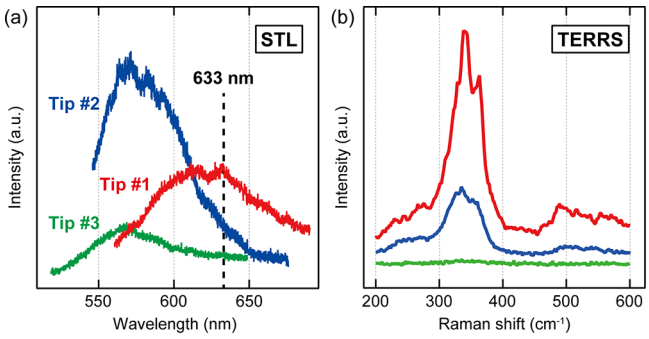


**Figure 2.** Physical enhancement mechanism examined under different tip conditions. (a) STL spectra obtained over the Ag(111) surface with three different Ag tips ($V_{bias}$ = 1 V, $I_t$ = 1 nA, $t_{exp}$ = 300 s, 78 K). (b) TERRS spectra obtained for 2-ML ZnO with the different tips ($\lambda_{ext}$ = 633 nm, $F$ = 0.34 mW$\mu m^{-2}$, $V_{bias}$ = 1 V, $I_t$ = 1 nA, $t_{exp}$ = 300 s, 78 K).

spectra obtained with different Ag tips exhibiting a different LSPR, although very similar STM images are acquired with them. In the next step, we recorded TERRS spectra on 2-ML ZnO with these tips (Figure 2b). A strong enhancement occurs for tip #1 whose LSPR is located around 630 nm, thus it can efficiently couple with the incoming and outgoing electromagnetic field at 633 nm excitation and eventually leads to a large enhancement. However, as expected, only a weak enhancement is observed for the off-resonance tips #2 and #3.

The local field enhancement is also dependent on the tip−surface distance. Figure 3a shows TERRS spectra recorded over a 2-ML ZnO at different gap distances. In this measurement, the tip approached toward the surface starting from an STM set-point of $V_{bias}$ = 1 V and $I_t$ = 1 nA. The TERRS intensity increases with decreasing the gap distance (down to −0.4 nm) but considerably decreases at smaller



DOI: 10.1021/acs.nanolett.9b02345
Nano Lett. 2019, 19, 5725−5731

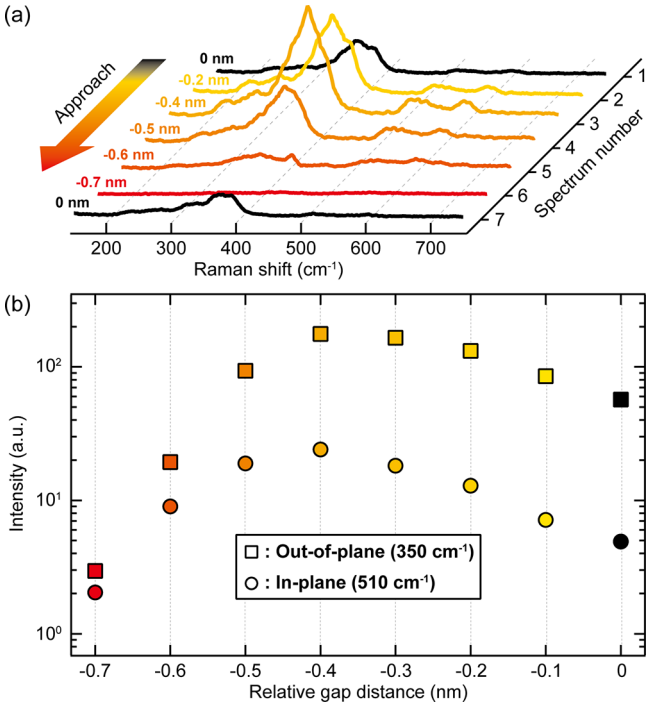


**Figure 3.** Gap distance dependence of TERRS. (a) TERRS spectra recorded on 2-ML ZnO at different gap distances relative to the STM set-point of $V_{bias}$ = 1 V and $I_t$ = 1 nA (Ag tip, $\lambda_{ext}$ = 633 nm, $F$ = 0.25 mW $\mu m^{-2}$, $t_{exp}$ = 90 s, 78 K). $V_{bias}$ is set to zero during the TERRS measurements. The spectra are recorded sequentially from the farthest distance and remeasured at the retracted position ($V_{bias}$ = 1 V and $I_t$ = 1 nA) after acuisition of Spectrum #6 (the smallest gap distance). (b) Raman intensity at ∼350 and ∼510 $cm^{-1}$ is plotted as a function of the relative tip−surface distance.

distances (Figure 3b). This behavior can be explained by quenching of the capacitive coupling mode (bonding dimer plasmon) due to quantum mechanical effects in plasmonic nanocavities.[22−26] Thus, at very short gap distances the LSPR observed in Figure 2a is suppressed, leading to the significant reduction of the TERRS signal. To rule out that the decrease of the TERRS intensity originates from large tip modifications, we recorded spectrum #7 in Figure 3a at the same STM set-point as spectrum #1 ($V_{bias}$ = 1 V and $I_t$ = 1 nA) after the approach sequence from spectrum #1 to #6. Spectrum #7 almost recovers its original shape. We also confirmed that the ZnO surface remained intact by imaging the same area before and after the TERRS measurement. The slight change between spectrum #1 and #7 may be attributed to subtle (atomic-scale) modification of the tip apex. We repeatedly observed the reduction of the TERRS intensity at short gap distances with different tips (see Supporting Information). At relatively large gap distances, the TERRS intensity monotonically decreases with distance (see Supporting Information).

We now turn to the chemical enhancement mechanism. In order to examine this, we made use of the slight difference in the electronic structures between 2- and 3-ML ZnO.[12,14] It was found that the TERRS signal is very weak (unobservable in most cases) on 3-ML ZnO with 633 nm excitation. Figure 4a shows a line scan of the TERRS spectra recorded across a single step of the ZnO layer, where the signal rapidly decreases and eventually disappears from 2- to 3-ML ZnO. On the other hand, with 780 nm excitation the TERRS signal can be obtained only from the 3-ML ZnO (see Supporting Information). Moreover, no Raman signal is observed with 532 nm excitation for both 2- and 3-ML ZnO. This pronounced excitation-wavelength dependence indicates the crucial role of chemical enhancement determined by resonances in electronic structures. The corresponding STS spectra (Figure 4b) show that the unoccupied state of the respective ZnO layers is observed at different onset voltages, that is, $V_{bias}$ = 1.8 and 1.4 V for 2- and 3-ML ZnO, respectively. Furthermore, the Shockley surface state of Ag(111) becomes an interface state of ZnO/Ag(111) and its onset is observed at $V_{bias}$ = −0.2 V, shifted from the value of the bare Ag surface (−0.07 V).[27] A similar change of a surface state has been observed on Cu(111).[28] Figure 4c depicts the electronic structure of the ZnO/Ag(111) interface to explain the chemical enhancement mechanism. The calculated electron effective mass of (0.24−0.27)$m_e$ in the conduction band of the free-standing 2-ML ZnO (see Supporting Information) is comparable with that in the surface state of the clean Ag(111) surface (∼0.28 $m_e$),[29] where $m_e$ is the electron mass. Hence the dispersion of these states may be similar for ultrathin ZnO

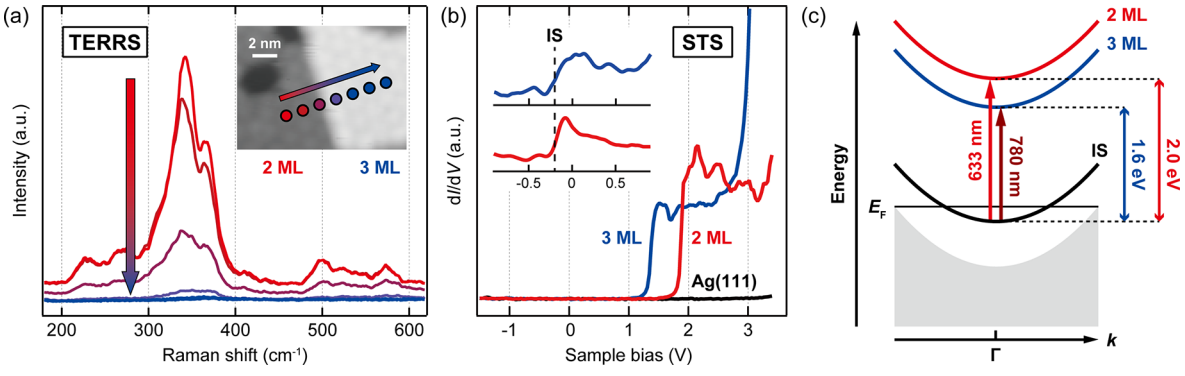


**Figure 4.** Chemical enhancement mechanism examined using 2- and 3-ML ZnO. (a) TERRS spectra recorded across a step between 2- and 3-ML ZnO (Ag tip, $\lambda_{ext}$ = 633 nm, $F$ = 0.38 mW $\mu m^{-2}$, $V_{bias}$ = 1 V, $I_t$ = 1 nA, $t_{exp}$ = 60 s, 78 K). The inset shows the STM image of the measurement area and the recorded locations are marked by the colored dots. (b) STS spectra of 2- and 3-ML ZnO and the Ag(111) surface measured in the constant height mode (the gap distance is fixed at $V_{bias}$ = 1 V and $I_t$ = 300 pA). The inset shows the magnified spectra near the Fermi level where the interface state (IS) is observed. The data are extracted from ref 14. (c) Schematic electronic structure of ZnO/Ag(111) around Γ-point. The energy difference between the IS and the conduction band edge of the ZnO layers is indicated. $E_F$, Fermi level of Ag(111). The gray region represents the projected bulk electronic states.



DOI: 10.1021/acs.nanolett.9b02345
Nano Lett. 2019, 19, 5725−5731

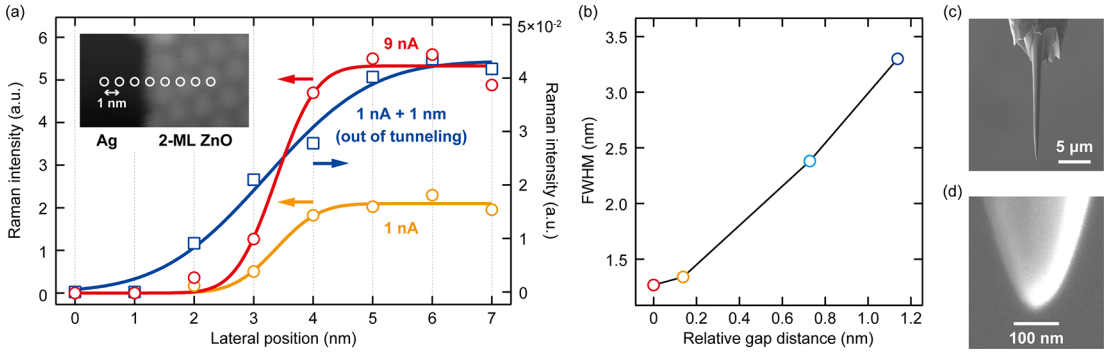


**Figure 5.** Spatial resolution of TERRS at a different tip−surface distance. (a) Raman intensity of the peak at ∼350 $cm^{-1}$ recorded across the step edge of the 2-ML ZnO at different gap distances (Au tip, $\lambda_{ext}$ = 633 nm, $F$ = 0.39 mW $\mu m^{-2}$, $V_{bias}$ = 1 V, $t_{exp}$ = 60 s, 78 K). The gap distance is set by the tunneling current indicated in the figure. The data are fitted by a step function broadened by a Gauss function (solid curve). (b) fwhm obtained from (b) is plotted as a function of the relative gap distance. The zero-point in the horizontal axis corresponds to the STM set-point of $V_s$ = 1 V and $I_t$ = 9 nA. (c,d) SEM micrographs of an Au tip that is shaped by FIB.

layers on Ag(111). The resonance in the chemical enhancement mechanism should occur around the Γ-point because it is suppressed by quantum interference at a large wave vector.[30] The excitation wavelengths of 633 and 780 nm (photon energies of 1.96 and 1.59 eV) match the vertical transition between the interface state and the conduction band of the 2- and 3-ML ZnO, respectively, whereas the 532 nm excitation (2.33 eV) is off-resonance for both layers. These observations are all consistent with the proposed resonant enhancement mechanism including the resonance between the interface state and the conduction band of the ZnO layers.

Next we examine the spatial resolution of TERRS at different tip−surface distances. Figure 5a shows the Raman intensity at ∼350 $cm^{-1}$ recorded across the edge of 2-ML ZnO on Ag(111). The lateral distributions of the Raman intensity are fitted with a step function convoluted with a Gaussian profile to estimate the spatial resolution. As shown in Figure 5b, we find that the full width at half-maximum (i.e., spatial resolution) varies significantly at relatively large tip−surface distances ($d_{gap} \gtrsim 1$ nm), wheras the variation becomes rather small and approaches ∼1 nm at short distances (in the tunneling regime). A similar spatial resolution of about 1 nm in the tunneling regime has been observed at the edge of two-dimensional silicene[31] and borophene[32] layers on Ag(111) and at a boundary of a molecular layer with two different tautomers.[33] However, the tip−surface distance dependence of the spatial resolution has not been reported so far.

The spatial resolution of TERRS should be associated with the effective volume of field confinement in the junction. Recent theoretical studies have proposed that atomic-scale features in subnanometric plasmonic cavities lead to extreme field confinement as a consequence of an atomistic lightning rod effect.[34,35] In experiment, we used Au or Ag tips sharpened by focused ion beam (FIB) milling,[36] which yields a sharp apex with an extremely smooth surface as seen in the scanning electron micrographs (Figure 5c,d). However, it is an accepted idea that the tip apex has atomic-scale protrusions that endow atomic resolution of the STM. Such atomistic structures may be created and modified by in situ tip-forming procedures, that is, applying short voltage pulses and poking the tip into a clean Ag surface in a controlled manner. Qualitative insight into the field enhancement in such an STM junction can be obtained by classical electrodynamic simulations using a simplified model, namely a spherical tip with a single nanoprotrusion above a flat Ag surface as discussed in ref 37 (see also Supporting Information for our simulations).

According to theoretical predictions, when the gap size of a plasmonic nanocavity becomes below ∼1 nm, quantum mechanical effects such as nonlocal screening and electron tunneling start affecting the frequency and lifetime of the LSPR as well as the local field enhancement.[22−26] Recent simulations by Urbieta et al. revealed that the effective volume of the confined field ($V_{eff}$) is also subject to quantum effects but the classical description can capture the main features of nanoscale field confinement at distances $d_{gap} \gtrsim 4$ Å.[35] In this regime, both quantum and classical simulations show a monotonic decrease of $V_{eff}$ when the gap distance of the nanocavity is reduced. At small gap distances, however, a continuous and rapid decrease of $V_{eff}$ occurs in classical simulations, whereas in the full-quantum simulation the variation of $V_{eff}$ becomes rather small as compared to the classical prediction and even increases for $d_{gap} \lesssim 3$ Å.[35] The latter behavior appears to be more consistent with our observation that the variation of the spatial resolution becomes small in the tunneling rang (Figure 5b). Therefore, quantum mechanical effects may be essential to gain further insight into the distance dependence of the spatial resolution. It should also be noted that the spatial resolution is affected by the tip conditions (see Supporting Information). This can be qualitatively explained by the size of the nanoprotrusion at the apex which determines the near-field confinement. Thus, improved tip shaping may allow us to attain the subnanometer resolution. According to a very recent report by Apkarian and co-workers,[38] atomic-resolution TERS of an adsorbed porphyrin derivative occurs in a contact regime ($d_{gap} \approx 2$ Å) where the charge transfer plasmon modes dominate the optical properties[24] and strong hybridization of the tip state with the molecule is expected. Therefore, in this regime the Raman scattering mechanism may be fundamentally different from our case.

In general, atomic-scale features on the tip apex are expected to be unstable at elevated temperatures, which most probably hampers the ultrahigh resolution of TERS at room temperature. In addition, the tip apex condition (structure) is readily modified at very small tip−surface distances. We believe that the stability of such atomistic structures at the tip apex is of fundamental importance to attain ultrahigh (Ångstrom) spatial resolution, which can be largely improved at cryogenic temperatures below <10 K.[38]



DOI: 10.1021/acs.nanolett.9b02345
Nano Lett. 2019, 19, 5725−5731

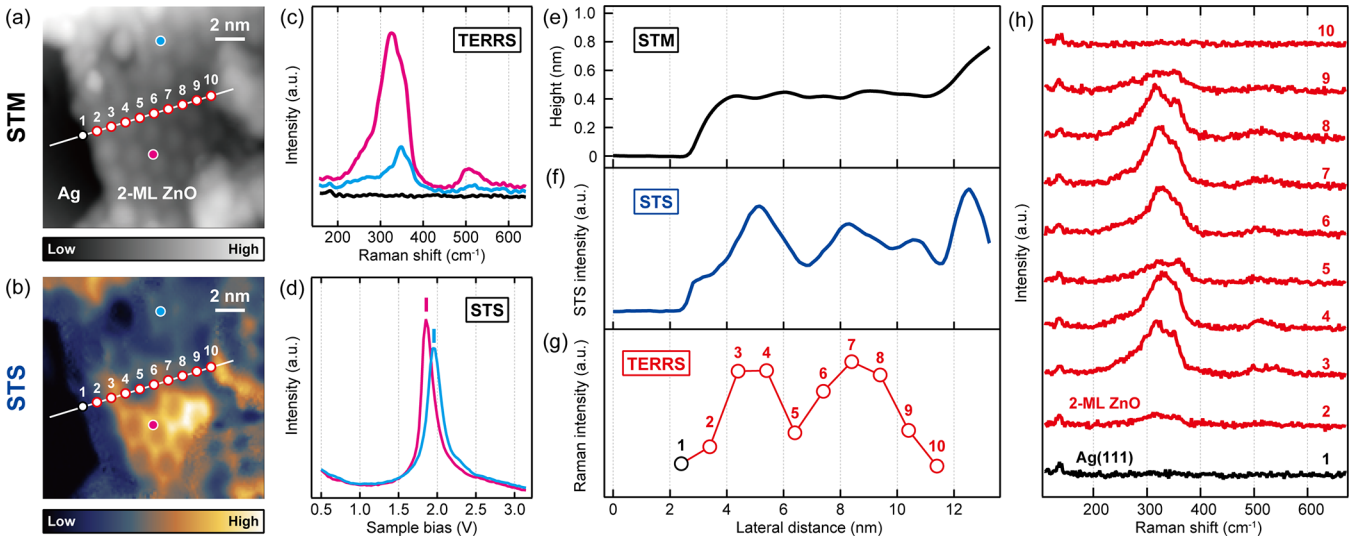


**Figure 6.** Correlation of the TERRS signal and the local electronic structure. (a,b) STM image and STS mapping over 2-ML ZnO/Ag(111) ($V_{bias}$ = 1.8 V and $I_t$ = 1 nA). (c) TERRS spectra obtained with an Au tip over the Ag(111) surface (black) and two different locations of the 2-ML ZnO indicated by the cyan and magenta markers in (a) and (b) (Au tip, $\lambda_{ext}$ = 633 nm, $F$ = 0.34 mW$\mu$m$^{-2}$, $V_{bias}$ = 1 V, $I_t$ = 1 nA, $t_{exp}$ = 20 s, 78 K). (d) Single-point STS recorded in the constant current mode at $I_t$ = 500 pA. (e,f) Profiles of the topographic height and the STS mapping along the white line in (a,b). (g) TERRS intensity at 325 cm$^{-1}$ obtained along the line and the recorded positions are indicated by the circles in (a,b). (h) TERRS spectra at different locations.

Finally, we examine in more detail the correlation between the local electronic structure and TERRS on 2-ML ZnO. Figure 6a,b display the STM image of the measurement area and the corresponding STS mapping at $V_{bias}$ = 1.8 V, respectively. The STS mapping reveals an inhomogeneous spatial distribution of the electronic structure over 2-ML ZnO. Figure 6c shows TERRS spectra obtained at two different locations as indicated by the magenta and cyan circles in Figure 6a,b. The TERRS intensity is much larger at the former location where the STS intensity at $V_{bias}$ = 1.8 V is higher (Figure 6b) than that of the latter location. A single-point STS measurement (Figure 6d) reveals that the conduction band edge is slightly different at these two locations. Note that the STS was recorded in constant current mode in order to highlight the conduction band edges of the ZnO layer. The observed differences of the conduction band edges result from a slightly different incommensurate structure between the ZnO layer and the Ag surface.[12] On the other hand, the Moiré pattern occurs due to a different STS intensity, thus a modulation of the local electronic density but the position of the conduction band edges remain the same.[14] Therefore, the TERRS intensity does not vary significantly at different positions on the Moiré pattern (see Supporting Informaton). These results also corroborate the resonance model in Figure 6c. We also carried out a line scan of the TERRS signal. Figure 6e–g are the profile of the topographic height, the STS intensity and the TERRS intensity at ~350 cm$^{-1}$, respectively, recorded along the line indicated in Figure 6a,b. Although the topographic height is relatively featureless on the terrace of 2-ML ZnO, the STS and the TERRS intensity exhibit significant modulations. The latter two signals show a pronounced correlation. Figure 6h shows the TERRS spectra obtained along the line indicated in Figure 6a,b.

In summary, we demonstrated that the resonance Raman scattering in TERS is correlated with the local electronic structure of the sample. Strong Raman signals of the ultrathin ZnO layers on a Ag(111) surface were obtained when both physical and chemical enhancement mechanism are operative. It was found that the spatial resolution of TERRS depends on the tip–surface distance and reaches ~1 nm in the tunneling regime. In combination with STS, the correlation between the TERRS intensity and the local DOS is resolved. Our results explicitly show that a confined electromagnetic field can interact with local electronic resonances at the (sub)nanometer scale.

**Methods.** All experiments were performed in an ultrahigh vacuum chamber (base pressure <5 × 10$^{-10}$ mbar) equipped with a low-temperature STM (modified UNISOKU USM-1400) operated with a Nanonis SPM controller. The bias voltage ($V_{bias}$) was applied to the sample with the tip at ground. All measurements were performed at 78 K. The Ag(111) surface was cleaned by repeated cycles of Ar$^+$ sputtering and annealing up to 670 K. The ultrathin ZnO layers were grown by a reactive deposition method as described in ref 29. The STM tips were made from polycrystalline Au and Ag wires by electrochemical etching. We further processed the tips by a FIB milling technique (FEI Helios NanoLab G3 FIB-SEM DualBeam system) to fabricate an extremely sharp tip with a nanoscopically smooth surface. The tips were cleaned under UHV conditions by Ar$^+$ sputtering before measurement. The cleanness of the apex was confirmed by measuring TERS spectrum over the clean Ag(111) surface. The laser beam (532 nm, solid-state laser; 633 nm, HeNe laser; 780 nm, solid-state laser) was focused to the STM junction using an in situ Ag-coated parabolic mirror (numerical aperture of ~0.6) mounted on the cold STM stage. The spot diameter on the tip apex was estimated to be about 3 $\mu$m. The beam alignment and focusing were performed precisely with piezo motors (Attocube GmbH) attached to the parabolic mirror, which allow three translational and two rotational motions of the parabolic mirror. The incident light was linearly polarized along the tip axis. The Raman signal was collected by the same parabolic mirror and detected outside of the UHV chamber with a grating spectrometer (Andor



DOI: 10.1021/acs.nanolett.9b02345
Nano Lett. 2019, 19, 5725–5731

Shamrock 303i). The STS ($dI/dV$) signal was recorded using a lock-in amplifier with a modulation voltage of 20 $mV_{rms}$ at 983 Hz.

## ■ ASSOCIATED CONTENT

### Supporting Information

The Supporting Information is available free of charge on the ACS Publications website at DOI: 10.1021/acs.nanolett.9b02345.

Far-field Raman spectrum of ultrathin ZnO layers on Ag(111), details of density functional theory calculations, phonon band structure of a free-standing 2-ML ZnO layer, calculated structure of 2-ML ZnO/Ag(111), electronic structure of a free-standing 2-ML ZnO, reduction of the TERRS intensity at a short gap distance observed for different tips, TERRS at relatively large gap distances, TERRS spectra recorded with 780 nm excitation, electrodynamic simulations of the field enhancement in the STM junction, spatial resolution of TERS with different tips, TERRS spectra measured at different sites in the Moiré pattern (PDF)

## ■ AUTHOR INFORMATION


### Corresponding Author

*E-mail: kuma@fhi-berlin.mpg.de.

### ORCID

Ikutaro Hamada: 0000-0001-5112-2452

Takashi Kumagai: 0000-0001-7029-062X


### Notes

The authors declare no competing financial interest.

## ■ ACKNOWLEDGMENTS

The authors thank Robert Schlögl for his generous support to implement the SEM measurement and the FIB fabrication of Au and Ag tips. T.K. acknowledges the support by JST-PRESTO (JPMJPR16S6). T.K. and M.W. acknowledge the support by the Deutsche Forschungsgemeinschaft through Sfb951. The numerical calculations were performed using the Numerical Materials Simulator at National Institute for Materials Science.

## ■ REFERENCES


(1) Jeanmaire, D. L.; van Duyne, R. P. Surface raman spectroelectrochemistry: Part I. Heterocyclic, aromatic, and aliphatic amines adsorbed on the anodized silver electrode. *J. Electroanal. Chem. Interfacial Electrochem.* **1977**, *84*, 1−20.

(2) Kneipp, K.; Wang, Y.; Kneipp, H.; Perelman, L. T.; Itzkan, I.; Dasari, R. R.; Feld, M. S. Single Molecule Detection Using Surface-Enhanced Raman Scattering (SERS). *Phys. Rev. Lett.* **1997**, *78*, 1667−1670.

(3) Pettinger, B.; Schambach, P.; Villagómez, C. J.; Scott, N. Tip-Enhanced Raman Spectroscopy: Near-Fields Acting on a Few Molecules. *Annu. Rev. Phys. Chem.* **2012**, *63*, 379−399.

(4) Pozzi, E. A.; Goubert, G.; Chiang, N.; Jiang, N.; Chapman, C. T.; McAnally, M. O.; Henry, A.-I.; Seideman, T.; Schatz, G. C.; Hersam, M. C.; van Duyne, R. P. Ultrahigh-Vacuum Tip-Enhanced Raman Spectroscopy. *Chem. Rev.* **2017**, *117*, 4961−4982.

(5) Verma, P. Tip-Enhanced Raman Spectroscopy: Technique and Recent Advances. *Chem. Rev.* **2017**, *117*, 6447−6466.

(6) Anderson, M. S. Locally enhanced Raman spectroscopy with an atomic force microscope. *Appl. Phys. Lett.* **2000**, *76*, 3130−3132.

(7) Hayazawa, N.; Inouye, Y.; Sekkat, Z.; Kawata, S. Metallized tip amplification of near-field Raman scattering. *Opt. Commun.* **2000**, *183*, 333−336.

(8) Stockle, R. M.; Suh, Y. D.; Deckert, V.; Zenobi, R. Nanoscale chemical analysis by tip-enhanced Raman spectroscopy. *Chem. Phys. Lett.* **2000**, *318*, 131−136.

(9) Zhang, R.; Zhang, Y.; Dong, Z. C.; Jiang, S.; Zhang, C.; Chen, L. G.; Zhang, L.; Liao, Y.; Aizpurua, J.; Luo, Y.; Yang, J. L.; Hou, J. G. Chemical mapping of a single molecule by plasmon-enhanced Raman scattering. *Nature* **2013**, *498*, 82−86.

(10) Chiang, N.; Jiang, N.; Chulhai, D. V.; Pozzi, E. A.; Hersam, M. C.; Jensen, L.; Seideman, T.; van Duyne, R. P. Molecular-Resolution Interrogation of a Porphyrin Monolayer by Ultrahigh Vacuum Tip-Enhanced Raman and Fluorescence Spectroscopy. *Nano Lett.* **2015**, *15*, 4114−4120.

(11) Tallarida, N.; Lee, J.; Apkarian, V. A. Tip-Enhanced Raman Spectromicroscopy on the Angstrom Scale: Bare and CO-Terminated Ag Tips. *ACS Nano* **2017**, *11*, 11393−11401.

(12) Shiotari, A.; Liu, B.-H.; Jaekel, S.; Grill, L.; Shaikhutdinov, S.; Freund, H.-J.; Wolf, M.; Kumagai, T. Local Characterization of Ultrathin ZnO Layers on Ag(111) by Scanning Tunneling Microscopy and Atomic Force Microscopy. *J. Phys. Chem. C* **2014**, *118*, 27428−27435.

(13) Tusche, C.; Meyerheim, H. L.; Kirschner, J. Observation of Depolarized ZnO(0001) Monolayers: Formation of Unreconstructed Planar Sheets. *Phys. Rev. Lett.* **2007**, *99*, 026102.

(14) Kumagai, T.; Liu, S.; Shiotari, A.; Baugh, D.; Shaikhutdinov, S.; Wolf, M. Local electronic structure, work function, and line defect dynamics of ultrathin epitaxial ZnO layers on a Ag(111) surface. *J. Phys.: Condens. Matter* **2016**, *28*, 494003.

(15) Liu, S.; Shiotari, A.; Baugh, D.; Wolf, M.; Kumagai, T. Enhanced resolution imaging of ultrathin ZnO layers on Ag(111) by multiple hydrogen molecules in a scanning tunneling microscope junction. *Phys. Rev. B: Condens. Matter Mater. Phys.* **2018**, *97*, 195417.

(16) Demiroglu, I.; Bromley, S. T. Evidence for multi-polymorphic islands during epitaxial growth of ZnO on Ag(111). *J. Phys.: Condens. Matter* **2016**, *28*, 224007.

(17) Moskovits, M. Surface selection rules. *J. Chem. Phys.* **1982**, *77*, 4408−4416.

(18) Moskovits, M.; Suh, J. S. Surface selection rules for surface-enhanced Raman spectroscopy: calculations and application to the surface-enhanced Raman spectrum of phthalazine on silver. *J. Phys. Chem.* **1984**, *88*, 5526−5530.

(19) Peng, C.; Qin, G.; Zhang, L.; Zhang, G.; Wang, C.; Yan, Y.; Wang, Y.; Hu, M. Dependence of phonon transport properties with stacking thickness in layered ZnO. *J. Phys. D: Appl. Phys.* **2018**, *51*, 315303.

(20) Zha, X.; Zhang, R.-q.; Lin, Z. Tuning thermal expansions of zinc oxide sheets by varying the layer thickness. *Europhys. Lett.* **2014**, *107*, 26007.

(21) Berndt, R.; Gimzewski, J. K.; Johansson, P. Inelastic tunneling excitation of tip-induced plasmon modes on noble-metal surfaces. *Phys. Rev. Lett.* **1991**, *67*, 3796−3799.

(22) Zuloaga, J.; Prodan, E.; Nordlander, P. Quantum Description of the Plasmon Resonances of a Nanoparticle Dimer. *Nano Lett.* **2009**, *9*, 887−891.

(23) Savage, K. J.; Hawkeye, M. M.; Esteban, R.; Borisov, A. G.; Aizpurua, J.; Baumberg, J. J. Revealing the quantum regime in tunnelling plasmonics. *Nature* **2012**, *491*, 574−577.

(24) Esteban, R.; Borisov, A. G.; Nordlander, P.; Aizpurua, J. Bridging quantum and classical plasmonics with a quantum-corrected model. *Nat. Commun.* **2012**, *3*, 825.

(25) Zhu, W.; Crozier, K. B. Quantum mechanical limit to plasmonic enhancement as observed by surface-enhanced Raman scattering. *Nat. Commun.* **2014**, *5*, 5228.

(26) Kravtsov, V.; Berweger, S.; Atkin, J. M.; Raschke, M. B. Control of plasmon emission and dynamics at the transition from classical to quantum coupling. *Nano Lett.* **2014**, *14*, 5270−5275.




DOI: 10.1021/acs.nanolett.9b02345
*Nano Lett.* 2019, 19, 5725−5731

(27) Li, J.; Schneider, W.-D.; Berndt, R.; Bryant, O. R.; Crampin, S. Surface-State Lifetime Measured by Scanning Tunneling Spectroscopy. *Phys. Rev. Lett.* **1998**, *81*, 4464−4467.
(28) Repp, J.; Meyer, G.; Rieder, K.-H. Snell's Law for Surface Electrons: Refraction of an Electron Gas Imaged in Real Space. *Phys. Rev. Lett.* **2004**, *92*, 036803.
(29) Kevan, S. D.; Gaylord, R. H. High-resolution photoemission study of the electronic structure of the noble-metal (111) surfaces. *Phys. Rev. B: Condens. Matter Mater. Phys.* **1987**, *36*, 5809−5818.
(30) *Topics in Applied Physics, Light Scattering in Solids*; Cardona, M., Ed.; Springer-Verlag, 1975.
(31) Sheng, S.; Wu, J.-b.; Cong, X.; Li, W.; Gou, J.; Zhong, Q.; Cheng, P.; Tan, P.-h.; Chen, L.; Wu, K. Vibrational Properties of a Monolayer Silicene Sheet Studied by Tip-Enhanced Raman Spectroscopy. *Phys. Rev. Lett.* **2017**, *119*, 196803.
(32) Sheng, S.; Wu, J.-B.; Cong, X.; Zhong, Q.; Li, W.; Hu, W.; Gou, J.; Cheng, P.; Tan, P.-H.; Chen, L.; Wu, K. Raman Spectroscopy of Two-Dimensional Borophene Sheets. *ACS Nano* **2019**, *13*, 4133−4139.
(33) Mahapatra, S.; Ning, Y.; Schultz, J. F.; Li, L.; Zhang, J.-L.; Jiang, N. Angstrom Scale Chemical Analysis of Metal Supported *Trans*- and *Cis*-Regioisomers by Ultrahigh Vacuum Tip-Enhanced Raman Mapping. *Nano Lett.* **2019**, *19*, 3267.
(34) Barbry, M.; Koval, P.; Marchesin, F.; Esteban, R.; Borisov, A. G.; Aizpurua, J.; Sánchez-Portal, D. Atomistic Near-Field Nanoplasmonics: Reaching Atomic-Scale Resolution in Nanooptics. *Nano Lett.* **2015**, *15*, 3410−3419.
(35) Urbieta, M.; Barbry, M.; Zhang, Y.; Koval, P.; Sánchez-Portal, D.; Zabala, N.; Aizpurua, J. Atomic-Scale Lightning Rod Effect in Plasmonic Picocavities: a Classical View to a Quantum Effect. *ACS Nano* **2018**, *12*, 585−595.
(36) Böckmann, H.; Liu, S.; Müller, M.; Hammud, A.; Wolf, M.; Kumagai, T. Near-Field Manipulation in a Scanning Tunneling Microscope Junction with Plasmonic Fabry-Pérot Tips. *Nano Lett.* **2019**, *19*, 3597−3602.
(37) Trautmann, S.; Aizpurua, J.; Götz, I.; Undisz, A.; Dellith, J.; Schneidewind, H.; Rettenmayr, M.; Deckert, V. A classical description of subnanometer resolution by atomic features in metallic structures. *Nanoscale* **2017**, *9*, 391−401.
(38) Lee, J.; Crampton, K. T.; Tallarida, N.; Apkarian, V. A. Visualizing vibrational normal modes of a single molecule with atomically confined light. *Nature* **2019**, *568*, 78−82.



DOI: 10.1021/acs.nanolett.9b02345
*Nano Lett.* 2019, 19, 5725−5731